Aggregated Shapley effects: nearest-neighbor estimation procedure and confidence intervals. Application to snow avalanche modeling

María Belén Heredia, Clémentine Prieur, Nicolas Eckert

Aggregated Shapley effects: nearest-neighbor estimation procedure and confidence intervals. Application to snow avalanche modeling.

María Belén Heredia
Univ. Grenoble Alpes, INRAE, UR ETNA, Grenoble, France

Clémentine Prieur
Univ. Grenoble Alpes, CNRS, Inria, Grenoble INP, LJK, Grenoble, France

Nicolas Eckert
Univ. Grenoble Alpes, INRAE, UR ETNA, Grenoble, France

Abstract

Dynamic models are simplified representations of some real-world entities that change over time. They are essential analytical tools with significant applications, e.g., in environmental and social sciences. The outputs produced by dynamic models are typically time and/or space dependent. Due to physical constraints, their parameters cannot be considered as independent from each others. Also, they can be significantly sensitive to variations of input parameters. A global sensitivity analysis (GSA) consists in modeling input parameters by a probability distribution which propagates through the model to the outputs. Then, input parameters are ordered according to their contribution on the model outputs by computing sensitivity measures. In this paper, we extend Shapley effects, a sensitivity measure well suited for dependent input parameters, to the framework of dynamic models. We also propose an algorithm to estimate the so-called aggregated Shapley effects and to construct bootstrap confidence intervals for the estimation of scalar and aggregated Shapley effects. We measure the performances of the estimation procedure and the accuracy of the probability of coverage of the bootstrap confidence intervals on toy models. Finally, our procedure is applied to perform a GSA of an avalanche flow dynamic model, for which the input/output sample is obtained from an acceptance-rejection algorithm. More precisely, we analyze the sensitivity in two different settings: (i) little knowledge on the input parameter probability distribution, and (ii) well-calibrated input parameter distribution. Probative linkages between local slope

and sensitivity indices demonstrate the usefulness of our approach for practical problems.

1 Introduction

Dynamic models are simplified representations of some real-world entity that change over time, in equations or computer code. These models are useful for the analysis of real-world phenomena, e.g., in environmental or social sciences Irwin and Wang [2017]. For a better understanding of a phenomenon or for forecasting purposes, it might be important to identify which input parameters entering in the formulation of such dynamic models are influential on the outputs of interest. Determining these influential parameters is one aim of global sensitivity analysis (GSA). A global sensitivity analysis (GSA) consists in modeling unknown input parameters by a probability distribution which propagates through the model to the outputs. Then, input parameters are ordered according to their contribution on the model outputs by computing sensitivity measures. In the literature, there exists different global sensitivity measures, e.g., variance based measures such as Sobol' indices Sobol' [1993], Owen [2014], density based measures Borgonovo [2007], Borgonovo et al. [2016], Veiga [2015], entropy measures Auder and B. [2008], etc. A review of global sensitivity measures can be found in, e.g., Borgonovo and Plischke [2016] or Iooss and Lemaître [2015].

Due to modeling constraints inherent to many applications, model input parameters might be dependent. It happens indeed that input parameters are interrelated by physical constraints, as for example in Radaideh et al. [2019] modeling the response of a nuclear reactor. In López-Benito and Bolado-Lavín [2017], the input parameters of a natural gas transmission model are sampled from an acceptance-rejection algorithm thus cannot be considered as independent (see also Kucherenko et al. [2017]). A particularity of dynamic models considered in this paper is that the output they produce are typically time and/or space dependent (see e.g., Alexanderian et al. [2020], Lamboni et al. [2011]). More specifically, the application that motivated our study is an avalanche flow dynamic model (Naaim et al. [2004]) which produces three outputs: the functional flow velocity and depth and the scalar runout distance, and depends on some poorly known inputs Eckert et al. [2008b]. This model is employed for elaborating land-use maps or for designing defense structures Naaim et al. [2010], Favier et al. [2014a]. Understanding the influence of input parameters on the model outputs is important for a better comprehension of avalanche phenomenon and for

determining the most influential parameter on which effort should be concentrated. Within a long-term forecasting context (see Section 6), avalanche samples are obtained from an acceptation-rejection algorithm thus (i) input parameters are dependent, (ii) input parameters are not necessarily confined in a rectangular region and (iii) input parameters have unknown probability distribution. For these reasons, we develop a GSA which can handle complex input parameter probability distributions and functional outputs (or multivariate outputs if we discretize functional ones).

Although the independence assumption on input parameters is unrealistic in many applications, it is traditionally required to interpret or to compute sensitivity measures. In other words, if input parameters are dependent, some sensitivity measures are difficult to interpret. E.g., if input parameters are dependent, the functional ANOVA decomposition used for the interpretation of Sobol' indices is not unique and Sobol' indices can actually sum to greater than one. Some authors have proposed strategies to estimate variance based sensitivity measures if input parameters are dependent (cite, e.g., Xu and Gertner [2008], Li et al. [2010], Chastaing et al. [2012], Mara and Tarantola [2012], Kucherenko et al. [2012], Mara et al. [2015], Zhang et al. [2015], Xu [2013], Hart and Gremaud [2018]). However, these papers do not provide an univocal way of partitioning the influence of input parameters on the output. In Jacques et al. [2006], grouped Sobol' indices are introduced. Grouped Sobol' indices can be defined if the input parameters can be splitted in independent groups of dependent parameters, then a Sobol' index is attributed to each group, but not to each input parameter. Other authors have proposed alternative sensitivity measures such as moment independent sensitivity measures (see, e.g., Borgonovo [2007]) or have adapted existing procedures to the framework of dependent input parameters (see, e.g., the screening procedure presented in Ge and Menendez [2017]). A more complete review of this literature can be found in Iooss and Prieur [2019].

The Shapley effects are a variance based sensitivity measure proposed by Owen [2014], which is meaningful in the framework of dependent input parameters Owen and Prieur [2017]. This measure is based on the Shapley value which is a cooperative game theory concept. Briefly speaking, Shapley value ensures a fair distribution of a gain among team players according to their individual contributions. As a sensitivity measure, Owen [2014] adapted the Shapley value into the Shapley effects by considering model input parameters as players and the gain function as the output variance. The main advantage of such an approach is that it is possible to attribute a non negative sensitivity index to each parameter, and the sum of the indices

is equal to one Broto et al. [2020], Iooss and Prieur [2019].

Regarding the estimation of the Shapley effects, Song et al. [2016], Broto et al. [2020] and Plischke et al. [2020] proposed estimation algorithms. Song et al. [2016] proposed two estimators for Shapley effects. Benoumechiara, Nazih and Elie-Dit-Cosaque, Kevin [2019] proposed bootstrap confidence intervals for Song et al. [2016] estimators. Plischke et al. [2020] proposed an estimation algorithm based on the Möbious inverse to reduce estimation computational cost. In fact, it is well known that Shapley effects estimation is costly. In the algorithm proposed in Song et al. [2016], it is assumed that it is possible to sample from the distribution of a subset of the input parameters conditionally to the complementary set of input parameters. In Broto et al. [2020], the authors proposed given data estimators based on nearest-neighbor, which can be computed from an i.i.d. sample of input parameters, which is in general more convenient for real applications. It is worth to mention that given data estimators of Sobol' indices have also been proposed in the literature: we can cite the EASI spectral method of Plischke [2010], Plischke et al. [2013] which relies on the notion of class-conditional densities, the nonparametric estimation methods of Da Veiga and Gamboa [2013] or Solís [2019], the fully Bayesian given data procedure proposed by Antoniano-Villalobos et al. [2019], and more recently in Gamboa et al. [2020] estimators based on rank statistics. But even if Sobol' indices estimation is available when input parameters are dependent, their interpretation is still difficult. Shapley effects have been studied in other works, e.g., Iooss and Prieur [2019] analyzed the effect of linear correlation between Gaussian inputs on the Shapley effects. Shapley effects have been also used in real application e.g., in a nuclear application where inputs are correlated Radaideh et al. [2019], and in the multi-physic coupling modeling of a rod ejection accident in a pressurized water reaction Delipei [2019]. Finally, Rabitti and Borgonovo [2019] extended Shapley effects to also provide information about input interactions.

In this work, we extend Shapley effects to multivariate or functional outputs in the framework of dependent input parameters. When outputs are multivariate or functional, it is possible to compute a sensitivity Shapley effect for each component of the output. However this approach leads to results that are difficult to interpret Alexanderian et al. [2020] or particularly redundant if we consider the case of discretized functional outputs Lamboni et al. [2009]. Lamboni et al. [2009] and Gamboa et al. [2013] extended Sobol' indices to multivariate or functional outputs. Alexanderian et al. [2020] extended Sobol' indices to time-dependent outputs. Following these papers, we introduce and study the properties of what we call aggregated Shapley

effects. If the output dimension is high (as it is the case, e.g., when considering the discretization of a functional output), a dimension reduction can be applied as a preliminary step to estimate efficiently aggregated Shapley effects. We use the Karhunen-Love (KL) expansion as in Lamboni et al. [2009], Alexanderian et al. [2020]. More precisely to perform KL expansion, we use the functional principal component analysis proposed by Yao et al. [2005]. The extension of Shapley effects to multivariate outputs has been early studied in Delipei [2019], but here we analyze more deeply its definition, properties and estimation. We also provide a bootstrap algorithm to estimate confidence intervals for scalar and aggregated Shapley effects motivated by Benoumechiara, Nazih and Elie-Dit-Cosaque, Kevin [2019]. Eventually, we perform the GSA of our avalanche flow dynamic model in two different settings: (i) little knowledge on the input parameter probability distribution, and (ii) well-calibrated input parameter distribution (Eckert et al. [2010]).

The paper is organized as follows. In Section 2, aggregated Shapley effects and their main properties are described. In Section 3, we propose an estimator for aggregated Shapley effects in a given data framework by extending the Monte-Carlo nearest-neighbor estimator of scalar Shapley effects introduced in Broto et al. [2020]. At the end of the section, we describe the functional principal components analysis algorithm to perform model dimension reduction proposed by Yao et al. [2005]. In Section 4, we propose a bootstrap algorithm to construct confidence intervals of the scalar and aggregated Shapley effect estimations based on Benoumechiara, Nazih and Elie-Dit-Cosaque, Kevin [2019]. In Section 5, we test our estimation procedure on two toy models: a multivariate linear Gaussian model and the mass-spring model. Finally in Section 6, our GSA procedure is applied to our avalanche dynamic model. We discuss our conclusions and perspectives in Section 7.

2 Aggregated Shapley effects

Shapley effects are sensitivity measures to quantify input importance proposed by Owen [2014]. These measures are particularly useful when inputs are dependent. Shapley effects are based in the concept of Shapley value, introduced in the framework of game theory Shapley [1953], which consists into dividing a game gain among a group of players in an equitable way. As sensitivity measures, Shapley effects consider model inputs as players and output variance as game function. Shapley effects can be naturally extended

to multivariate output models by following the ideas presented in Gamboa et al. [2013] and Lamboni et al. [2009] to generalize Sobol' indices to multivariate output models (see also Alexanderian et al. [2020] for time-dependent models). We call these new sensitivity measures aggregated Shapley effects.

2.1 Definition

Let us define $\mathbf{Y} = (Y_1, \ldots, Y_j, \ldots, Y_p) = f(\mathbf{X})$ the p multivariate output of a model f that depends on d random inputs $\mathbf{X} = (X_1, \ldots, X_d)$. The inputs are defined on some probability space $(\Omega, \mathcal{F}, \mathbb{P}_{\mathbf{X}})$ and $f \in \mathbb{L}^2(\mathbb{P}_{\mathbf{X}})$. For any $\mathfrak{u} \subseteq \{1, \ldots, d\}$, let us define $-\mathfrak{u} = \{1, \ldots, d\} \setminus \mathfrak{u}$ its complement. We set $\mathbf{X}_{\mathfrak{u}} = (X_i)_{i \in \mathfrak{u}}$. Note that the inputs are not necessary independent. In the framework of our application to avalanche modeling, the model produces outputs of the form $\mathbf{Y} = (Y_1 = f(s_1, \mathbf{X}), \ldots, Y_p = f(s_p, \mathbf{X}))$, with $s_1, \ldots, s_p \in \mathbb{R}$ the p discretization points along the avalanche corridor.

In this section we recall the definition and main properties of the Shapley value, on which the definition of Shapley effects is based. Given a set of d players in a coalitional game and a charateristic function $\text{val} : 2^d \to \mathbb{R}$, $\text{val}(\emptyset) = 0$, the Shapley value $(\phi_1, \ldots, \phi_d)$ is the only distribution of the total gains $\text{val}(\{1, \ldots, d\})$ to the players satisfying the desirable properties listed below:

1. (Efficiency) $\sum_{i=1}^{d} \phi_i = \text{val}(\{1, \ldots, d\})$.
2. (Symmetry) If $\text{val}(\mathfrak{u} \cup \{i\}) = \text{val}(\mathfrak{u} \cup \{\ell\})$ for all $\mathfrak{u} \subseteq \{1, \ldots, d\} - \{i, j\}$, then $\phi_i = \phi_\ell$.
3. (Dummy) If $\text{val}(\mathfrak{u} \cup \{i\}) = \text{val}(\mathfrak{u})$ for all $\mathfrak{u} \subseteq \{1, \ldots, d\}$, then $\phi_i = 0$.
4. (Additivity) If val and val' have Shapley values ϕ and ϕ' respectively, then the game with characteristic function val + val' has Shapley value $\phi_i + \phi'_i$ for $i \in \{1, \ldots, d\}$.

It is proved in Shapley [1953] that according to the Shapley value, the amount that player i gets given a coalitional game (val, d) is:

$$\phi_i = \frac{1}{d} \sum_{\mathfrak{u} \subseteq -\{i\}} \binom{d-1}{|\mathfrak{u}|}^{-1} (\text{val}(\mathfrak{u} \cup \{i\}) - \text{val}(\mathfrak{u})) \ \ \forall i \in \{1, \ldots, d\}. \quad (1)$$

The Shapley value also satisfies the linearity property:

5. (Linearity) Let $\lambda \in \mathbb{R}$, if λval and val have Shapley values ϕ' and ϕ, then $\phi'_i = \lambda\phi_i$ for all $i \in \{1, \ldots, d\}$.

The linearity property is used to prove some of the nice properties of aggregated Shapley effects (see Propositions 1 and 2 further).

The Shapley effects are defined by considering the characteristic function of the game as:

$$\text{val}_j(\mathfrak{u}) = \frac{\text{Var}\left(\mathbb{E}(Y_j|\mathbf{X}_\mathfrak{u})\right)}{\text{Var}(Y_j)},\ \mathfrak{u} \subseteq \{1, \ldots, d\} \tag{2}$$

in Equation (1). Thus, the scalar Shapley effect of input i in output j is defined as:

$$Sh_i^j = \frac{1}{d\,\text{Var}(Y_j)} \sum_{\mathfrak{u} \subseteq -\{i\}} \binom{d-1}{|\mathfrak{u}|}^{-1} \left(\text{Var}\left(\mathbb{E}(Y_j|\mathbf{X}_{\mathfrak{u}\cup i})\right) - \text{Var}\left(\mathbb{E}(Y_j|\mathbf{X}_\mathfrak{u})\right)\right). \tag{3}$$

Shapley effects can be naturally extended to models with multivariate outputs following ideas from Gamboa et al. [2013] and Lamboni et al. [2009] where authors proposed to extend Sobol' indices to multivariate outputs. Aggregated Shapley effect of an input i is then defined as:

$$GSh_i = \frac{\sum_{j=1}^p \text{Var}(Y_j) Sh_i^j}{\sum_{j=1}^p \text{Var}(Y_j)}, \tag{4}$$

where Sh_i^j is the scalar Shapley effect of input X_i in output Y_j. This sensitivity measure is a weighted sum of the scalar Shapley effects where weights correspond to the proportion of the variance of each output over the sum of all individual variances.

2.2 Properties

In this section, we prove some nice properties of aggregated Shapley effects.

Proposition 1. *The aggregated Shapley effects GSh_i, $i \in \{1, \ldots, d\}$, correspond to the Shapley value with characteristic function defined as:*

$$val(i) = \frac{\sum_{j=1}^p Var(Y_j)\, val_j(i)}{\sum_{j=1}^p Var(Y_j)}. \tag{5}$$

Proof. The proof is straightforward. It is a direct consequence of the linearity and additivity properties of the Shapley value. Let $i \in \{1, \dots, d\}$ and $j \in \{1, \dots, p\}$. The characteristic function val_j (see Equation 2) has Shapley value Sh_i^j, $i \in \{1, \dots, d\}$. Thanks to the linearity and additivity properties (see properties 4. and 5. of the Shapley value), the characteristic function $\frac{\sum_{j=1}^p \mathrm{Var}(Y_j)\mathrm{val}_j(i)}{\sum_{i=1}^p \mathrm{Var}(Y_j)}$ leads to the Shapley value $\frac{\sum_{j=1}^p \mathrm{Var}(Y_j)Sh_i^j}{\sum_{i=1}^p \mathrm{Var}(Y_j)}$. □

The characteristic function (5) can be written in matricial form:

$$\mathrm{val}(i) = \frac{\sum_{j=1}^p \mathrm{Var}(Y_j)\mathrm{val}_j(i)}{\sum_{i=1}^p \mathrm{Var}(Y_j)} = \frac{\sum_{j=1}^p \mathrm{Var}(\mathbb{E}(Y_j|X_i))}{\sum_{i=1}^p \mathrm{Var}(Y_j)} = \frac{tr(\Sigma_i)}{tr(\Sigma)} \qquad (6)$$

where Σ_i is the covariance matrix of $\mathbb{E}(\mathbf{Y}|X_i)$ and Σ is the covariance matrix of $\mathbf{Y}$. Note that the characteristic function val of aggregated Shapley effects corresponds to the definition of the aggregated Sobol' indices introduced in Lamboni et al. [2009], Gamboa et al. [2013]. In the next proposition, we prove that aggregated Shapley effects accomplish the natural requirements for a sensitivity measure mentioned in Proposition 3.1 in Gamboa et al. [2013].

Proposition 2. *Let $i \in \{1, \dots d\}$. The following items hold true.*

i. $0 \leq GSh_i \leq 1$.

ii. *GSh_i is invariant by left-composition by any nonzero scaling of f, which means, for any $\lambda \in \mathbb{R}$, the aggregated Shapley effect GSh'_i of $\lambda f(\boldsymbol{X})$ is GSh_i.*

iii. *GSh_i is invariant by left-composition of f by any isometry of $\mathbb{R}^p$, which means, for any $O \in \mathbb{R}^{p\times p}$ such that $O^tO = I$, the aggregated Shapley effect GSh'_i of $Of(\boldsymbol{X})$ is GSh_i for all $i \in \{1, \dots, d\}$.*

Proof. *i.* As for all $j \in \{1, \dots, p\}$ $0 \leq Sh_i^j \leq 1$ and as the sum of the non negative weights $\mathrm{Var}(Y_j)/\sum_{\ell=1}^p \mathrm{Var}(Y_\ell)$ is one, we deduce that $0 \leq GSh_i \leq 1$. *ii.* Note that GSh'_i can be written as $GSh'_i = \frac{\sum_{j=1}^p \mathrm{Var}(\lambda Y_j)Sh_i^{'j}}{\sum_{j=1}^p \mathrm{Var}(\lambda Y_j)}$, where $Sh_i^{'j}$ is the Shapley effect associated to the characteristic function val'_j. Notice that $\mathrm{val}'_j(i) = \frac{\mathrm{Var}(\mathbb{E}(\lambda Y_j|X_i))}{\mathrm{Var}(\lambda Y_j)} = \mathrm{val}_j(i)$. Thus, $Sh_i^{'j} = Sh_i^j$ from where $GSh'_i = GSh_i$ which means the aggregated Shapley effect is invariant by any nonzero scaling of f. *iii.* Let us write $g(\mathbf{X}) = Of(\mathbf{X}) = O\mathbf{Y} = \mathbf{U}$. The

characteristic function associated to the aggregated Shapley effect GSh'_i of $\mathbf{U}$ is then (see Equation eq. (6)) val'$(i) = tr(\Sigma_i^{\mathbf{U}})/tr(\Sigma^{\mathbf{U}})$ where $\Sigma_i^{\mathbf{U}}$ is the covariance matrix of $\mathbb{E}(\mathbf{U}|X_i)$ and $\Sigma^{\mathbf{U}}$ is the covariance matrix of $\mathbf{U}$. Then,

$$\text{val'}(i) = \frac{tr(\Sigma_i^{\mathbf{U}})}{tr(\Sigma^{\mathbf{U}})} = \frac{tr(O\Sigma_i^{\mathbf{Y}}O^t)}{tr(O\Sigma^{\mathbf{Y}}O^t)} = \frac{tr(\Sigma_i^{\mathbf{Y}})}{tr(\Sigma^{\mathbf{Y}})} = \text{val}(i).$$

As val(i) has an unique Shapley value GSh_i, val$'(i)$ has Shapley value GSh_i which proves that $GSh'_i = GSh_i$ for all $i \in \{1, \dots, d\}$. □

In this section, we have proven that aggregated Shapley effects are sensitivity measures. In the next section, we describe the estimation procedure we propose for aggregated Shapley effects, based the estimation procedure of scalar Shapley effects proposed in [Broto et al., 2020, Section 6] when observing an i.i.d. sample of $(\mathbf{X}, \mathbf{Y})$. Such a procedure, which does not require a specific form for the design of experiments is also called given data procedure.

3 Estimation procedure for scalar and aggregated Shapley effects

The aggregated Shapley effect estimation procedure we propose in this section is based on the given data estimation procedure of the scalar Shapley effects introduced in [Broto et al., 2020, Section 6.1.1.]. In the application we consider in Section 6, samples are constructed using acceptance-rejection rules. Therefore the standard pick-freeze estimation procedure (see, e.g., Janon et al. [2014]) can not be used as it is based on a specific pick-freeze type design of experiments. It is the reason why we turn to the given data estimation procedure of scalar Shapley effects introduced in [Broto et al., 2020, Section 6.1.1.]. For sake of clarity, we first present the estimation procedure for scalar Shapley effects in Section 3.1 before extending it to the estimation of aggregated Shapley effects in Section 3.2.

3.1 Double Monte Carlo given data estimation of scalar Shapley effects

As noticed in [Song et al., 2016, Theorem 1], replacing the characteristic function $\tilde{c}_j(\mathfrak{u}) = \text{Var}(\mathbb{E}(Y_j|\mathbf{X}_{\mathfrak{u}}))$ by the characteristic function $c_j(\mathfrak{u}) = \mathbb{E}(\text{Var}(Y_j|\mathbf{X}_{-\mathfrak{u}}))$ with $\mathfrak{u} \subseteq \{1, \dots, d\}$ in Equation eq. (3) does not change the definition of Shapley effects. Moreover, as pointed in Song et al. [2016]

(based on the work in Sun et al. [2011]), the double Monte Carlo estimator of $\tilde{c}_j(\mathfrak{u})$ can suffer from a non neglectable bias if the inner loop sample is small, while in contrast the double Monte Carlo estimator of $c_j(\mathfrak{u})$ is unbiased for any sample size. For that reason, we turn to the double Monte Carlo estimator of $c_j(\mathfrak{u})$. To estimate the scalar Shapley effects from the estimates of $c_j(\mathfrak{u})$, $\mathfrak{u} \subseteq \{1, \dots, d\}$, the two aggregation procedures are discussed in [Broto et al., 2020, Section 4], the random permutation aggregation procedure, and the subset aggregation procedure. We focus in this work on the subset aggregation procedure as it allows a variance reduction. Note that $c_j(\emptyset) = 0$ and that $c_j(\{1, \dots, d\}) = \mathrm{Var}(Y_j)$, which is assumed to be known in Broto et al. [2020], and that is estimated by the empirical variance in the present paper. As already mentioned, we consider the given data version for the subset aggregation procedure with double Monte Carlo introduced in [Broto et al., 2020, Section 6.1.1.] for the estimation of scalar Shapley effects. More precisely, given a n sample $(\mathbf{X}^{(i)}, \mathbf{Y}^{(i)})$, $1 \leq i \leq n$ of $(\mathbf{X}, \mathbf{Y})$, we define:

$$\widehat{c}_j(\mathfrak{u}) = \frac{1}{N_{\mathfrak{u}}} \sum_{\ell=1}^{N_{\mathfrak{u}}} \widehat{E}^j_{\mathfrak{u}, s_\ell} \text{ with} \tag{7}$$

$$\widehat{E}^j_{\mathfrak{u}, s_\ell} = \frac{1}{N_I - 1} \sum_{i=1}^{N_I} \left(f_j\left(\mathbf{X}^{(k_n^{-\mathfrak{u}}(s_\ell, i))}\right) - \frac{1}{N_I} \sum_{h=1}^{N_I} f_j\left(\mathbf{X}^{(k_n^{-\mathfrak{u}}(s_\ell, h))}\right) \right)^2 \tag{8}$$

with the notation $f_j(\mathbf{X}) = Y_j$. For $\emptyset \subsetneq \mathfrak{v} \subsetneq \{1, \dots, d\}$, the index $k_n^{\mathfrak{v}}(l, m)$ denotes as in [Broto et al., 2020, Section 6] the index such that $\mathbf{X}_{\mathfrak{v}}^{k_n^{\mathfrak{v}}(l,m)}$ is the (or one of the) m-th closest element to $\mathbf{X}_{\mathfrak{v}}^{(l)}$ in $(\mathbf{X}_{\mathfrak{v}}^{(i)})_{1 \leq i \leq n}$ and such that $(k_n^{\mathfrak{v}}(l, m))_{1 \leq m \leq N_I}$ are two by two distinct and $(s_\ell)_{1 \leq \ell \leq N_{\mathfrak{u}}}$ is a sample of uniformly distributed integers without replacement in $\{1, \dots, n\}$. N_I and N_u are respectively the Monte-Carlo sample sizes for the conditional variance and expectation. The choice of these two parameters is discussed further. In [Broto et al., 2020, Theorem 6.6.], it is proved that under theoretical assumptions, $\widehat{c}_j(\mathfrak{u})$ converges in probability to $c_j(\mathfrak{u})$ when n and $N_{\mathfrak{u}}$ go to ∞. The algorithm that consists in estimating scalar Shapley effects by plugging eq. (7) in Equation eq. (3) is called subset aggregation procedure:

$$\widehat{Sh}_i^j = \frac{1}{d\, \hat{\sigma}_j^2} \sum_{\mathfrak{u} \subseteq -i} \binom{d-1}{|\mathfrak{u}|}^{-1} \left(\widehat{c}_j(\mathfrak{u} \cup \{i\}) - \widehat{c}_j(\mathfrak{u})\right) \tag{9}$$

where $\hat{\sigma}_j^2$ is the empirical estimator of $\mathrm{Var}(Y_j)$. Note that, in the subset aggregation procedure, $N_{\mathfrak{u}}$ depends on each $\emptyset \subsetneq \mathfrak{u} \subsetneq \{1, \dots, d\}$.

Finally, we discuss the choice of N_I and $N_{\mathfrak{u}}$ for all $\emptyset \subsetneq \mathfrak{u} \subsetneq \{1, \dots, d\}$. We set as in Broto et al. [2020] $N_I = 3$ and we choose $N_{\mathfrak{u}}$ according to the rule proposed in [Broto et al., 2020, Proposition 4.2.] which aims at minimizing $\sum_{i=1}^{d} \mathrm{Var}(\widehat{Sh}_i^j)$ for a fixed total cost $\kappa \sum_{\emptyset \subsetneq \mathfrak{u} \subsetneq \{1,\dots,d\}} N_{\mathfrak{u}} = N_{tot}$ fixed by the user. Note that the optimal values $N_{\mathfrak{u}}^* = \left\lfloor N_{tot} \binom{d}{|\mathfrak{u}|}^{-1} (d-1)^{-1} \right\rfloor$, $\emptyset \subsetneq \mathfrak{u} \subsetneq \{1, \dots, d\}$, do not depend on $1 \leq j \leq p$. The optimal values $N_{\mathfrak{u}}^*$ are computed under theoretical assumptions that are not satisfied for the given data version of the estimators. However, numerical experiments in Broto et al. [2020] show that this choice performs well in practice. Note that the estimator cost in terms of number of model evaluations is n while the cost in terms of nearest-neighbors search is N_{tot}. In [Broto et al., 2020, Proposition 6.12.], it is proved that under theoretical assumptions the scalar Shapley effect estimators $\widehat{Sh}_i^j$ converge to the scalar Shapley effects in probability when n and N_{tot} go to ∞. Once more, although theoretical assumptions for the convergence are not guaranteed in the applications, numerical performance of the estimators have been demonstrated in Broto et al. [2020].

3.2 Estimator of the aggregated Shapley effects

Given scalar Shapley effect estimators whose definition is recalled in the previous section, we propose to estimate the aggregated Shapley effects by:

$$\widehat{GSh}_i = \frac{\sum_{j=1}^{p} \hat{\sigma}_j^2 \widehat{Sh}_i^j}{\sum_{j=1}^{p} \hat{\sigma}_j^2} = \frac{1}{d \sum_{j=1}^{p} \hat{\sigma}_j^2} \sum_{j=1}^{p} \sum_{\mathfrak{u} \subseteq -i} \binom{d-1}{|\mathfrak{u}|}^{-1} \left(\widehat{c}_j(\mathfrak{u} \cup \{i\}) - \widehat{c}_j(\mathfrak{u}) \right), \tag{10}$$

with $\hat{\sigma}_j^2$ the empirical estimator of $\mathrm{Var}(Y_j)$ and $\widehat{c}_j(\mathfrak{u})$ defined by (7).

3.3 Dimension reduction: functional principal component analysis

If model f is space or time-dependent, inspired by Alexanderian et al. [2020] and Lamboni et al. [2009], we perform a Karhunen-Loève (KL) expansion to obtain a low-rank model representation. In fact, aggregated Shapley effects might be computed more effectively in a low-rank representation. To perform KL expansion, we use the principal component analysis through conditional expectation (PACE) method proposed by Yao et al. [2005] (see also Antoniadis et al. [2012] for an illustration of its application). More precisely, we have a collection of n independent trajectories of a smooth

random function $f(.,\mathbf{X})$ with unknown mean $\mu(s) = \mathbb{E}(f(s,\mathbf{X})), s \in \tau$, where τ is a bounded and closed interval in $\mathbb{R}$, and covariance function $G(s_1,s_2) = \mathrm{Cov}(f(s_1,\mathbf{X}), f(s_2,\mathbf{X})), s_1, s_2 \in \tau$. We assume that G has a L^2 orthogonal expansion in terms of eigenfunction ξ_k and non increasing eigenvalues λ_k such that:

$$G(s_1,s_2) = \sum_{k\geq 1} \lambda_k \xi_k(s_1,\mathbf{X})\xi_k(s_2,\mathbf{X}), s_1, s_2 \in \tau.$$

The KL orthogonal expansion of $f(s,\mathbf{X})$ is:

$$f(s,\mathbf{X}) = \mu(s) + \sum_{k\geq 1} \alpha_k(\mathbf{X})\xi_k(s) \approx \mu(s) + \sum_{k=1}^{q} \alpha_k(\mathbf{X})\xi_k(s), s \in \tau, \qquad (11)$$

where $\alpha_k(\mathbf{X}) = \int_\tau f(s,\mathbf{X})\xi_k(s)ds$ is the k-th functional principal component (fPC) and q is a truncation level. For fPCs estimation, the authors in Yao et al. [2005] propose first to estimate $\hat{\mu}(s)$ using local linear smoothers and to estimate $\widehat{G}(s_1,s_2)$ using local linear surface smoothers (Fan and Gijbels [1996]). The estimates of eigenfunctions and eigenvalues correspond then to the solutions of the following integral equations:

$$\int_\tau \widehat{G}(s_1,s)\widehat{\xi}_k(s_1)ds_1 = \widehat{\lambda}_k\, \widehat{\xi}_k(s), s \in \tau,$$

with $\int_\tau \widehat{\xi}(s)ds = 1$ and $\int_\tau \widehat{\xi}_k(s)\widehat{\xi}_m(s) = 0$ for all $m \neq k \leq q$. The problem is solved by using a discretization of the smoothed covariance (see further details in Rice and Silverman [1991] and Capra and Müller [1997]). Finally, fPCs $\hat{\alpha}_k(\mathbf{X}) = \int_\tau f(s,\mathbf{X})\widehat{\xi}_k(s)ds$ are solved by numerical integration.

Aggregated Shapley effects are approximated using the low rank KL model representation with truncation level q, in other words, they are computed with only the q first fPCs:

$$\widetilde{GSh_i} = \frac{1}{d\sum_{k=1}^{q}\lambda_k} \sum_{k=1}^{q} \sum_{\mathfrak{u}\subseteq -i} \binom{d-1}{|\mathfrak{u}|}^{-1} \left(\mathbb{E}(\mathrm{Var}(\alpha_k(\mathbf{X})|\mathbf{X}_{\mathfrak{u}\cup\{i\}})) - \mathbb{E}(\mathrm{Var}(\alpha_k(\mathbf{X})|\mathbf{X}_{\mathfrak{u}}))\right). \qquad (12)$$

Remark eq. (12) can be estimated as eq. (10).

In unreported numerical test cases, we noticed that using the same sample to perform fPCA and to estimate the Shapley effects provides better results than splitting the sample in two parts.

4 Bootstrap confidence intervals with percentile bias correction

Confidence intervals are a valuable tool to quantify uncertainty in estimation. We consider non parametric bootstrap confidence intervals with bias percentile correction (see, e.g., Efron [1981], Efron and Tibshirani [1986]). More precisely, we propose to construct confidence intervals, with a block bootstrap procedure, following ideas in Benoumechiara, Nazih and Elie-Dit-Cosaque, Kevin [2019]. Indeed, bootstrap by blocks is necessary to preserve the nearest-neighbor structure in Equation eq. (8) and to avoid potential equalities in distance (see Assumption 6.3 in Broto et al. [2020]). We describe in algorithm 1 how to create B bootstrap samples for scalar Shapley effect estimators $\widehat{Sh}_i^j$ and aggregated Shapley effect estimators $\widehat{GSh}_i$, and then we describe the percentile bias correction method.

If model output is scalar, only Steps 1 to 3 of algorithm 1 should be used. The block bootstrap procedure is described by Steps 3.1 to 3.3. Also, the same sample $(\mathbf{x}, \mathbf{y})$ is used to estimate the variance of the outputs Y_j, $1 \leq j \leq p$, and the Shapley effects. In unreported numerical experiments, we noticed once more that using one sample gives better results than splitting the sample in two parts: one for estimating the variance of the outputs, and the other to estimate the Shapley effects.

For $1 \leq i \leq d$, $1 \leq j \leq p$, let $\mathcal{R}_i = \{\widehat{GSh}_i^{(1)}, \ldots, \widehat{GSh}_i^{(B)}\}$ and $\mathcal{R}_i^j = \{\widehat{Sh}_i^{j,(1)}, \ldots, \widehat{Sh}_i^{j,(B)}\}$, the bias-corrected percentile method presented in Efron and Tibshirani [1986] is applied. Let us denote by Φ the standard normal cumulative distribution function and by Φ^{-1} its inverse. A bias correction constant z_0, estimated as $\hat{z}_0 = \Phi^{-1}\left(\frac{\#\{\widehat{GSh}_i^{(b)} \in \mathcal{R}_i \text{ s. t. } \widehat{GSh}_i^{(b)} \leq \widehat{GSh}_i\}}{B}\right)$ is computed (similar for $\widehat{Sh}_i^j$). Then, the corrected quantile estimate $\hat{q}(\beta)$ for $\beta \in]0,1[$ is defined as $\hat{q}_i(\beta) = \Phi(2\hat{z}_0 + z_\beta)$, where z_β satisfies $\Phi(z_\beta) = \beta$. Corrected bootstrap confidence interval of level $1-\alpha$ is estimated by the interval whose endpoints are $\hat{q}_i(\alpha/2)$ and $\hat{q}_i(1-\alpha/2)$.

To guarantee the validity of the previous BC corrected confidence interval $[\hat{q}_i(\alpha/2), \hat{q}_i(1-\alpha/2)]$, there must exist an increasing transformation g, $z_0 \in \mathbb{R}$ and $\tau > 0$ such that $g(\widehat{GSh}_i) \sim \mathcal{N}(GSh_i - \tau z_0, \tau^2)$ and $g(\widehat{GSh}_i^*) \sim \mathcal{N}(\widehat{GSh}_i - \tau z_0, \tau^2)$ where $\widehat{GSh}_i^*$ is the bootstrapped $\widehat{GSh}_i$ for fixed sample (see Efron [1981]). Normality hypothesis can be tested using traditional normality tests as Shapiro test or using graphical methods as empirical normal quantile-quantile plots. In our application and test cases, we observed that

Algorithm 1 B bootstrap samples for $\widehat{Sh}_i^j$ and $\widehat{GSh}_i$

Inputs: (i) A n i.i.d. random sample $(\mathbf{x}^k, \mathbf{y}^k)_{k\in\{1,\dots,n\}}$ with $\mathbf{x}^k \in \mathbb{R}^d$ and $\mathbf{y}^k \in \mathbb{R}^p$. (ii) For each $\emptyset \subsetneq \mathfrak{u} \subsetneq \{1,\dots,d\}$, a $N_\mathfrak{u}$ random sample $(s_\ell)_{1\le\ell\le N_\mathfrak{u}}$ from $\{1,\dots,n\}$.

Outputs: B bootstrap samples for $\widehat{Sh}_i^j$ and $\widehat{GSh}_i$.

for $b = 1$ **to** $b = B$ **do**

1. Create a n bootstrap sample $\mathbf{y}^{(b)}$ by sampling with replacement from the rows of $\mathbf{y}$.
2. Compute, for $1 \le j \le p$, $\widehat{\sigma}_j^{2,(b)}$ the empirical variance of $\mathbf{y}_j^{(b)}$.
3. For each $j \in \{1,\dots,p\}$:
   3.1. For all $\mathfrak{u}$ and for all $(s_\ell)_{1\le\ell\le N_\mathfrak{u}}$ compute $\widehat{E}^j_{\mathfrak{u},s_\ell}$ using eq. (8).
   3.2. For all $\mathfrak{u}$, create a $N_\mathfrak{u}$ bootstrap sample $\widehat{E}^{j,(b)}_{\mathfrak{u},s_\ell}$ by sampling with replacement from $\left(\widehat{E}^j_{\mathfrak{u},s_\ell}\right)_{1\le\ell\le N_\mathfrak{u}}$ computed in Step 3.1.
   3.3. Compute $\widehat{c_j}^{(b)}(\mathfrak{u}) = \frac{1}{N_\mathfrak{u}} \sum_{\ell=1}^{N_\mathfrak{u}} \widehat{E}^{j,(b)}_{\mathfrak{u},s_\ell}$ for all $\mathfrak{u}$ using eq. (7).
   3.4. Compute the b bootstrap sample of $\widehat{Sh}_i^j$ according to eq. (9):

$$\widehat{Sh}_i^{j,(b)} = \frac{1}{d\,\widehat{\sigma}_j^{2,(b)}} \sum_{\mathfrak{u}\subseteq -i} \binom{d-1}{|\mathfrak{u}|}^{-1} \left(\widehat{c_j}^{(b)}(\mathfrak{u}\cup\{i\}) - \widehat{c_j}^{(b)}(\mathfrak{u})\right).$$

4. Compute the b bootstrap sample of $\widehat{GSh}_i$ using eq. (10):

$$\widehat{GSh}_i^{(b)} = \frac{1}{d\sum_{j=1}^p \widehat{\sigma}_j^{2,(b)}} \sum_{j=1}^{p} \sum_{\mathfrak{u}\subseteq -i} \binom{d-1}{|\mathfrak{u}|}^{-1} \left(\widehat{c_j}^{(b)}(\mathfrak{u}\cup\{i\}) - \widehat{c_j}^{(b)}(\mathfrak{u})\right).$$

end for

g can be chosen as the identity. To prove empirically the performance of the procedure described in algorithm 1, we compute the empirical probability of coverage (POC) of simultaneous intervals using Bonferroni correction. The POC with Bonferroni correction is the probability that the interval $[\hat{q}_i(\alpha/(2d)), \hat{q}_i(1-\alpha/(2d))]$ contains GSh_i for all $i \in \{1, \ldots, d\}$ simultaneously. To be more precise, if the confidence intervals are computed in N independent samples of size n of $(\mathbf{X}, \mathbf{Y})$. The POC is estimated as $\widehat{POC} = \sum_{k=1}^{N} \frac{w^k}{N}$, where w^k is equal to 1 if $\hat{q}_i(\alpha/(2d)) \leq GSh_i \leq \hat{q}_i(1-\alpha/(2d))$ for all i, and 0 otherwise.

5 Test cases

In this section, we numerically study the performance of the estimation procedure and the probability coverage of the boostrap confidence intervals we introduced in the previous section. We consider two test cases: a multivariate linear Gaussian model and the functional mass spring model proposed in the work of Gamboa et al. [2013]. To estimate the scalar Shapley effects, we use the function `shapleySubsetMc` of the `R` package `sensitivity` corresponding to the estimation procedure defined by (7), (8) and (9). Functional PCA is performed using the `R` package `FPCA` Chen et al. [2020].

5.1 Multivariate linear Gaussian model

We consider a multivariate linear model with two Gaussian inputs based on the example from Iooss and Prieur [2019]. For this toy function, there is an analytical expression of the scalar and aggregated Shapley effects (see Iooss and Prieur [2019]).

The model f is defined as $\mathbf{Y} = f(\mathbf{X}) = B^T\mathbf{X}$ with $\mathbf{X} \sim \mathcal{N}(\mu, \Gamma)$, $\Gamma \in \mathbb{R}^{d\times d}$ a positive-definite matrix and $\mathbf{B} \in \mathbb{R}^{d\times p}$. In this example, we consider $d = 2$ and $p = 3$ which means $\mathbf{Y} = (Y_1, Y_2, Y_3)$. The variance of the centered random variables X_1 and X_2 are equal to $\sigma_1^2 = 1$ and $\sigma_2^2 = 3$, respectively and their correlation $\rho = 0.4$. Thus the covariance matrix of $\mathbf{X}$ is given by:

$$\Gamma = \begin{bmatrix} \sigma_1^2 & \rho\sigma_1\sigma_2 \\ \rho\sigma_1\sigma_2 & \sigma_2^2 \end{bmatrix} = \begin{bmatrix} 1 & 0.69 \\ 0.69 & 3 \end{bmatrix},$$

and the coefficients of $B = (\beta_{ij}) \in \mathbb{R}^{2\times 3}$ are chosen as:

$$B = \begin{bmatrix} 1 & 4 & 0.1 \\ 1 & 3 & 0.9 \end{bmatrix}.$$

The variance of the output Y_j with $j \in \{1,2,3\}$ is $\sigma^2_{Y_j} = \beta^2_{1j}\sigma^2_1 + 2\rho\beta_{1j}\beta_{2j}\sigma_1\sigma_2 + \beta^2_{2j}\sigma^2_2$.

The scalar Shapley effects are:

$$\begin{aligned}
\sigma^2_{Y_j}\phi^j_1 &= \beta^2_{1j}\sigma^2_1\left(1-\frac{\rho^2}{2}\right) + \rho\beta_{1j}\beta_{2j}\sigma_1\sigma_2 + \beta^2_2\sigma^2_2\frac{\rho^2}{2}, \\
\sigma^2_{Y_j}\phi^j_2 &= \beta^2_{2j}\sigma^2_2\left(1-\frac{\rho^2}{2}\right) + \rho\beta_{1j}\beta_{2j}\sigma_1\sigma_2 + \beta^2_1\sigma^2_1\frac{\rho^2}{2}.
\end{aligned}$$

Then, the aggregated Shapley effects for $i \in \{1,2\}$ are calculated according to eq. (10).

First, we focus on scalar Shapley effect estimation and the associated confidence intervals, for example scalar Shapley effects for Y_1 output. For Y_1 output, the most important input is X_2 with a Shapley effect of 0.66. In fig. 1, we analyze estimation accuracy and POC evolution in function of n and N_{tot}. n and N_{tot} values are fixed according to our computation budget. For each combination of n and N_{tot}, $N = 300$ independent random samples are used. To estimate the bootstrap confidence intervals, we use $B = 500$ bootstrap samples. The 95% quantile of the absolute error are displayed. Scalar Shapley effects estimation depends on n and N_{tot}. As expected, bias decreases when n and N_{tot} increase. If n is fixed, bias decreases when N_{tot} increases. In particular, bias is the smallest with $n = 5000$ and $N_{tot} = 1000$. Regardless sample sizes, POCs estimated vary around 0.9 as expected.

The estimation of the bias for aggregated Shapley effects and the POC evolution by varying n and N_{tot} are displayed in fig. 2. Similarly as for scalar effects, POC is close to 0.9, regardless the sample size and, bias reduces when n and N_{tot} increase.

We estimate Shapley effects and aggregated Shapley effects if inputs correlation is higher ($\rho = 0.9$). POC and bias results are also satisfactory (not shown). In fact, POC values vary also around 0.9 and bias decreases and goes to 0 when n and N_{tot} increases. For this simple test case, we have shown that confidence intervals using algorithm 1 reach accurate coverage probability and that bias reduces when n and N_{tot} increase. Nevertheless in this test case, estimation is effortless because $d = 2$.

5.2 Mass-spring model

The method is illustrated on a test case with discretized functional output: the functional mass-spring model proposed by Gamboa et al. [2013], where

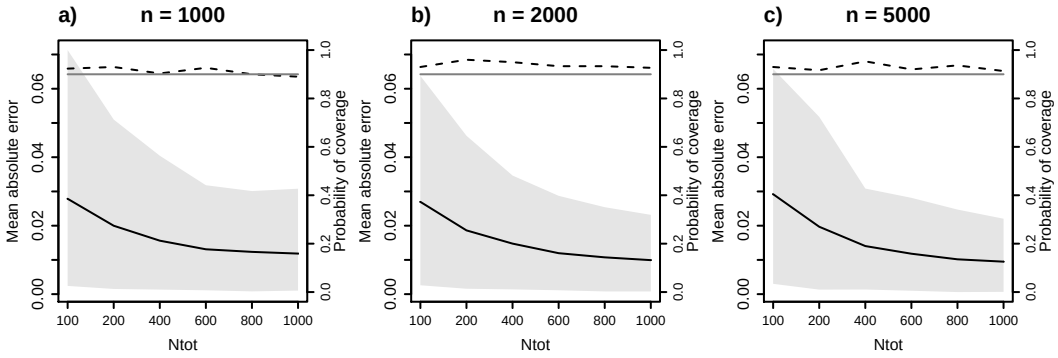

Figure 1: Linear Gaussian model: mean absolute error of the estimation of scalar Shapley effects of the output Y_1 in N=300 i.i.d. samples in function of N_{tot} using different sample sizes a) $n = 1000$, b) $n = 2000$ and c) $n = 5000$. The 0.05 and 0.95 pointwise quantiles of the absolute error are drawn with gray polygons. The probability of coverage of the 90% bootstrap simultaneous intervals is displayed with dotted lines. The theoretical probability of coverage 0.9 is also shown with a plain gray line. The bootstrap sample size is fixed to $B = 500$.

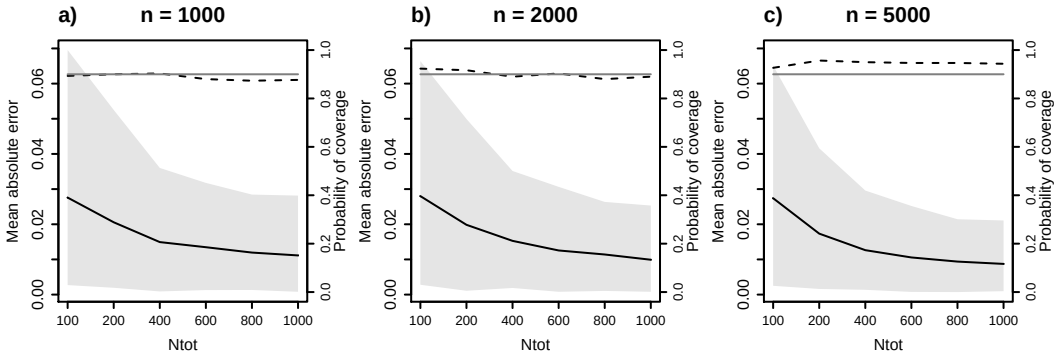

Figure 2: Linear Gaussian model: mean absolute error of the estimation of aggregated Shapley effects in N=300 i.i.d. samples in function of N_{tot} using different sample sizes a) $n = 1000$, b) $n = 2000$ and c) $n = 5000$. The 0.05 and 0.95 pointwise quantiles of the absolute error are drawn with gray polygons. The probability of coverage of the 90% bootstrap simultaneous intervals is displayed with dotted lines. The theoretical probability of coverage 0.9 is also shown with a gray plain line. The bootstrap sample size is fixed to $B = 500$.

Input	Description	Distribution
m	mass (kg)	$\mathcal{U}[10, 12]$
c	damping constant ($\mathrm{Nm}^{-1}\mathrm{s}$)	$\mathcal{U}[0.4, 0.8]$
k	spring constant (Nm^{-1})	$\mathcal{U}[70, 90]$
l	initial elongation (m)	$\mathcal{U}[-1, -0.25]$

Table 1: Mass spring model: Inputs description and uncertainty intervals. $\mathcal{U}$ denotes the uniform distribution.

the displacement of a mass connected to a spring is considered:

$$m\ell''(t) + c\ell'(t) + k\ell(t) = 0, \tag{13}$$

with initial conditions $\ell(0) = l$, $\ell'(0) = 0$, and $t \in [1, 40]$. There exists an analytical solution to Equation eq. (13). This model has four inputs (see more details in table 1). The model output is the vector $\mathbf{Y} = f(\mathbf{X}) = (\ell(t_1), \ldots, \ell(t_{800}))$, $\quad t_i = 0.05i$ with $i \in \{1, \ldots, 800\}$.

Inputs are considered independent. The true aggregated Shapley effects are unknown but they are approximated using a high sample size $n = 25\,000$ and $N_{tot} = 10\,000$. Then, the Shapley effects estimated are $\widehat{GS}_m = 0.38$, $\widehat{GS}_c = 0.01$, $\widehat{GS}_k = 0.51$ and, $\widehat{GS}_l = 0.09$. Given these results, inputs ranking is: k, m, l and c which corresponds to the same ranking obtained using Sobol' indices (see Table 3 of Gamboa et al. [2013]).

The discretized output is high-dimensional ($p = 800$). We perform fPCA (see Section 3.3) to estimate the effects using the first $q \ll p$ fPCs. fig. 3 shows the POC and bias evolution if different values for n and N_{tot} are used for the aggregated effects estimation. We use the first 6 fPCs which explain 95% of the output variance (see fig. 3 a). For each n and N_{tot} combination, the aggregated Shapley effects are estimated for $N = 100$ independent samples and confidence intervals are estimated with $B = 500$ bootstrap samples. Bias is large if sample size is small $n = 1000$ (see fig. 3 b). However, it reduces drastically when sample sizes increases as expected. In particular, if $n = 5000$ and $N_{tot} = 2002$ bias is the smallest (see fig. 3 d). If n and N_{tot} are too small, POC estimated values are lower than 0.9. This might be a consequence of bias in the estimation (see fig. 3 b). But when N_{tot} increases, POC is close to 0.9. In general in our experiments, confidence intervals are correct because POC values are around 0.9 when N_{tot} increases.

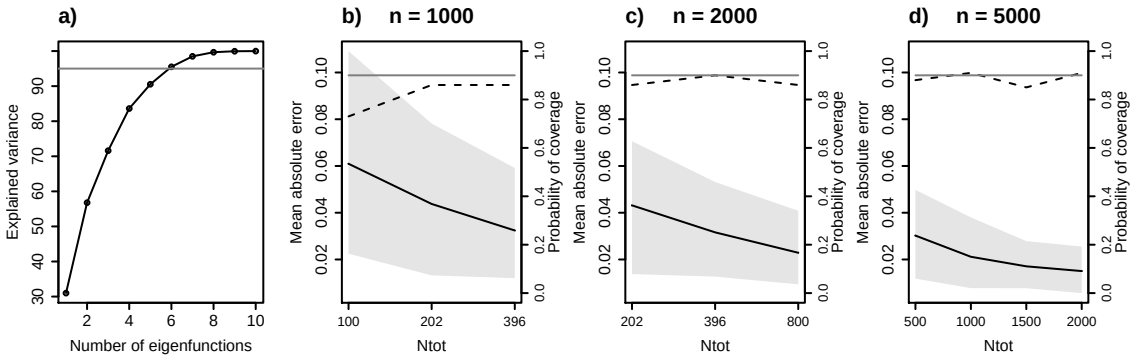

Figure 3: Mass spring model: a) Explained variance as a function of the decomposition basis size. The gray line is displayed at 95% of the variance explained which corresponds to 6 eigenfunctions. The mean absolute error of the estimation of aggregated Shapley effects using the first 6 eigenfunctions in $N = 100$ i.i.d. samples in function of N_{tot} using sample of size b) $n = 1000$, c) $n = 2000$ and d) $n = 5000$. The 0.05 and 0.95 pointwise quantiles of the absolute error are drawn with gray polygons. The probability of coverage of the 90% bootstrap simultaneous intervals is displayed with a dotted line. The 0.9 value is also highlighted with a plain gray line. The bootstrap sample size is fixed to $B = 500$.

6 Snow avalanche modeling

6.1 Model

Our avalanche model is based on depth-averaged Saint-Venant equations and considers the avalanche as a fluid in motion. In more detail, it considers only the dense layer of the avalanche. The flow depth is then small compared to its length. The model assumes the avalanche is flowing on a curvilinear profile $z = l(x)$, where z is the elevation and x is the projected distance measured from the top of the avalanche path. Under these assumptions, shallow-water approximations of the mass and momentum equations can be used:

$$\begin{aligned} \frac{\partial h}{\partial t} + \frac{\partial hv}{\partial x} &= 0 \\ \frac{\partial hv}{\partial t} + \frac{\partial}{\partial x}\left(hv^2 + \frac{h^2}{2}\right) &= h\left(g\sin\phi - \mathrm{F}\right) \end{aligned}$$

where $v = \|\vec{\mathbf{v}}\|$ is the flow velocity, h is the flow depth, ϕ is the local angle, t is the time, g is the gravity constant and $\mathrm{F} = \|\vec{\mathbf{F}}\|$ is a frictional force. The model uses the Voellmy frictional force $\mathrm{F} = \mu g cos\phi + \frac{g}{\xi h}v^2$, where μ and ξ are friction parameters. The equations are solved with a finite volumes scheme Naaim [1998].

The numerical model depends on six inputs: the friction parameters μ and ξ, the length $\mathrm{l_{start}}$ of the avalanche release zone, the snow depth $\mathrm{h_{start}}$ within the release zone, the abscissa corresponding to the beginning of the release zone denoted by $\mathrm{x_{start}}$ and the discretized topography of the flow path, denoted by $D = (\mathbf{x}, \mathbf{z}) \in \mathbb{R}^{N_s \times 2}$ where $\mathbf{x} \in \mathbb{R}^{N_S}$ is the vector of projected abscissa positions and $\mathbf{z} = l(\mathbf{x}) \in \mathbb{R}^{N_S}$ is the elevation vector. N_s is the number of points of the discretized path. We use for D the topography of a path located in Bessans, France. This particular path already considered in other works (Eckert et al. [2008a, 2010], Favier et al. [2014b], Eckert, Nicolas et al. [2018]) in well documented in the French avalanche database Bourova et al. [2016]. The model outputs are the flow velocity, flow depth trajectories in the path D and runout distance of an avalanche. Note that the model has two functional and one scalar outputs and these three outputs are the objects of the GSA study. We develop our GSA in two contexts or scenarios: (i) little knowledge on the input parameter probability distribution, and (ii) well-calibrated input parameter distribution.

Input	Description	Distribution
μ	Static friction coefficient	$\mathcal{U}[0.05, 0.65]$
ξ	Turbulent friction [m/s^2]	$\mathcal{U}[400, 10000]$
$\mathrm{l_{start}}$	Length of the release zone [m]	$\mathcal{U}[5, 300]$
$\mathrm{h_{start}}$	Mean snow depth in the release zone [m]	$\mathcal{U}[0.05, 3]$
$\mathrm{x_{start}}$	Release abscissa [m]	$\mathcal{U}[0, 1600]$

Table 2: Avalanche model, scenario 1: Input description and uncertainty intervals. In the the GSA, we consider $\mathrm{vol_{start}} = l_{start} \times h_{start} \times 72.3/\cos(35°)$ instead of $\mathrm{h_{start}}$ and $\mathrm{l_{start}}$.

6.2 Scenario 1

6.2.1 Principle

We first determine the most influential input parameters sampled from uniform distributions. We thus expect from the GSA a better understanding of the numerical model. Inputs μ and ξ vary in their physical value ranges. Inputs $\mathrm{l_{start}}$ and $\mathrm{h_{start}}$ vary in their spectrum of reasonable values given by the avalanche path characteristics. The $\mathrm{x_{start}}$ input distribution is determined by calculating the abscissa interval where the release zone average slope is superior to 30°. Indeed, the slope remains above 30° during the first 1600m of the path. A good approximation of avalanche release zones is commonly obtained this way. Since different studies (Bartelt et al. [2012], Brian Dade and Huppert [1998]) suggest that the volume of snow is a critical quantity that controls flow dynamics, we consider $\mathrm{vol_{start}}$ as input of the GSA instead of $\mathrm{h_{start}}$ and $\mathrm{l_{start}}$. The latter is evaluated as $\mathrm{vol_{start}} = l_{start} \times h_{start} \times 72.3/\cos(35°)$. The mean width and slope of the release zone equal to 72.3m and 35°, respectively. All uncertainty intervals are summed-up in table 2. The input correlations are close to 0 since we assume they are a priori independent.

For a given avalanche simulation, its functional velocity and flow depth outputs have a high number of zeros because they are null above the beginning of the release zone and after the runout position. Also, there might be some avalanche simulations that are meaningless in physical terms and/or not useful to assess the related risk. Therefore to perform GSA, we select simulations that accomplish the following acceptance-rejection (AR) rules: (i) avalanche simulation is flowing in the interval $[1600m, 2412m]$, (ii) its volume is superior to 7000 m^3 and, (iii) avalanche runout distance is inferior to 2500m which corresponds to the end of the path. The return period

of avalanches in the interval $[1600m, 2412m]$ varies from 1 to 10 000 years according to the work of Eckert et al. [2010]. Roughly speaking, a return period is the mean time in which a given runout distance is reached or exceeded at a given path's position Eckert et al. [2007, 2008b], Schläppy et al. [2014]. Also, we focus on medium, large and very large avalanches which have a high potential damage.

6.2.2 Global sensitivity analysis results

We first ran $n_0 = 100\,000$ avalanche simulations from an i.i.d. sample of input distributions described in table 2. Then, by applying (i) to (iii) our AR sample size was reduced to $n_1 = 6152$ (section 6.2.1). Even if the initial sample size is high ($n_0 = 100\,000$) and if the corresponding input parameter sample does not present any significant correlation structure, the AR sample size is low and we can observe a correlation structure. For example, inputs μ and ξ were independent for the initial sample but the correlation computed after the AR algorithm is 0.31. Note that the input parameter correlations induced by the AR algorithm were the main motivation to compute Shapley effects and not Sobol' indices in this first scenario.

On section 6.2.2 are plotted highest density region (HDR) boxplots for the velocity and flow depth, obtained by using the R package `rainbow` developed by Hyndman and Shang [2010]. The HDR boxplot is a vizualization tool for functional data based on the density estimation of the first two components of the PCA decomposition of the observed functions (see Hyndman [1996] for further details). In the studied interval, the avalanche velocity ranges from 0.1ms^{-1} to 71.56ms^{-1} and avalanches are decelerating (see section 6.2.2 a). Flow depths vary from 0.03m to 7.52m. The flow depth curves exhibit high fluctuations between $[2100m, 2300m]$ (see section 6.2.2 b) which corresponds to a region where path's topography is mostly convexe. Runout distances vary from 2409m to 2484m (see section 6.2.2 c).

On section 6.2.2 panels a and b, ubiquitous (pointwise) Shapley effects of velocity and flow depth curves are shown, respectively. Depending on the output, results are quite different. For velocity, x_{start} is the most relevant during a large part of the path but its importance decreases along the path and, conversely, the importance of the other inputs increases. For the flow depth output, the most important input is $\text{vol}_{\text{start}}$ since the corresponding Shapley effects vary from 0.4 to 0.2 along the path. Nevertheless, other inputs are not completely negligible. Input importance also varies according to the topography. In fact, the ubiquitous effect variation corresponds to local slope changes (see section 6.2.2 a and b). Correlations between ubiq-

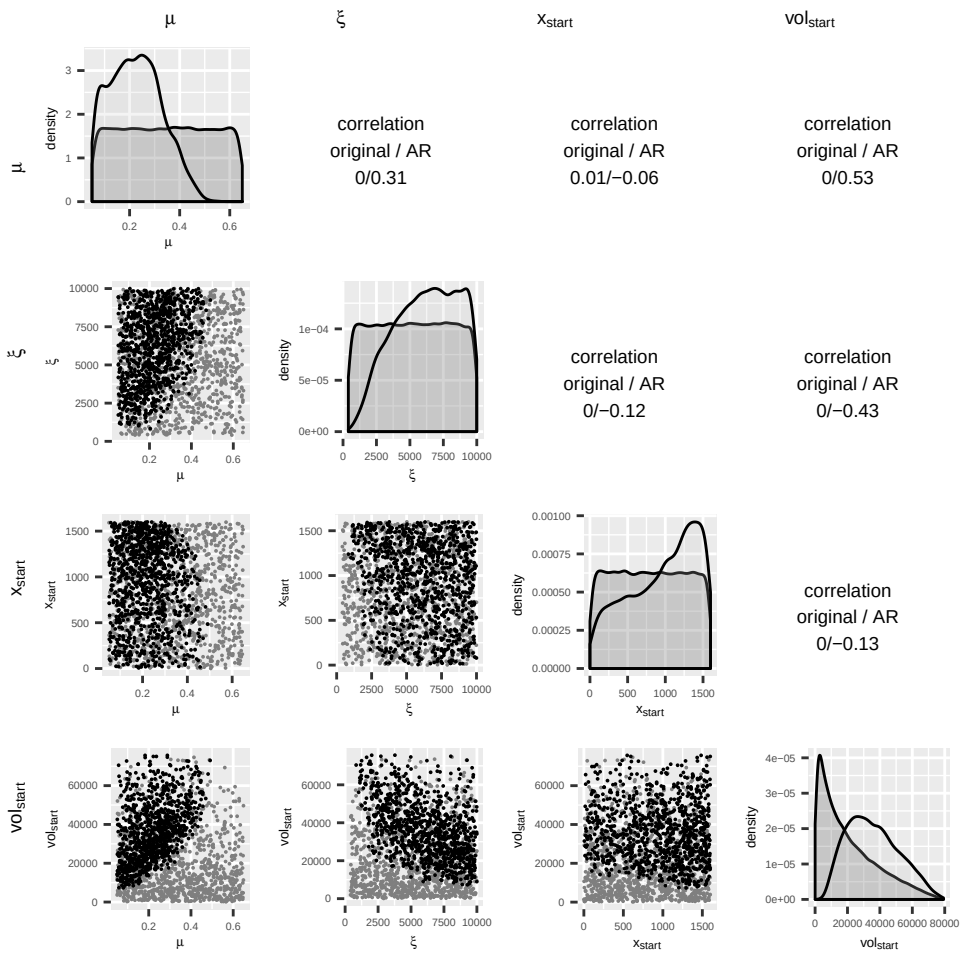

Figure 4: Avalanche model, scenario 1: scatter-plots of initial (black points) and acceptance rejection (gray points) samples. In the figure's diagonal, the density function of the initial (gray color) and AR (transparent) samples are displayed. Input correlations of the original and AR samples are shown. 1000 subsamples of original and AR samples are used for illustration purpose.

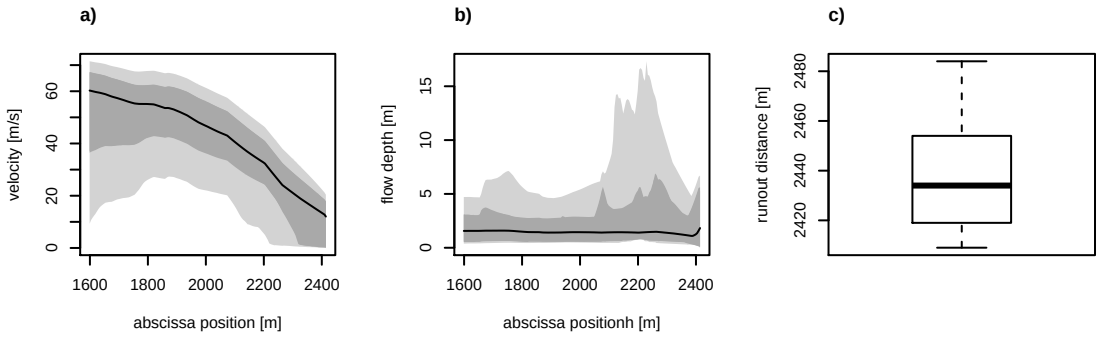

Figure 5: Avalanche model, scenario 1: a) and b) functional HDR boxplots of velocity and flow depth curves, resp. It is shown 50% HDR (light gray), 100% HDR(dark gray) and modal curve (black line). c) runout distance boxplot. The AR sample size is $n_1 = 6152$.

uitous effects and local slope have been computed and are rather high. For example, for the velocity, the absolute value of the correlation is higher than 0.51 for all input parameters. This implies that local slope changes play an important role on the input contribution to output variations, a nice results showing the relevance of the GSA analysis to understand the dynamical properties of the flow. Eventually, for runout distance, the four inputs are relevant.

section 6.2.2 shows aggregated Shapley effects and 90% confidence intervals computed over space intervals $[x, 2412]$ where $x \in \{1600, 1700, \ldots, 2412\}$. The aggregated effects are computed in the first fPCs explaining more than 95% of the output variance. Aggregated effects seem more robust than ubiquitous effects, specially in zones where local slope shows high variations (see section 6.2.2 compared to section 6.2.2). For explaining more than 95% of the velocity output variance, 2 fPCs are required, while, for explaining more than 95% of the flow depth output variance, at most 4 fPCs are required, depending on x. For the velocity output, the most important input is $\mathrm{x_{start}}$ in the interval $[1600m, 2100m]$ but its importance decreases along the path. In the interval $[2017m, 2412m]$ where return periods are non trivial, $\mathrm{x_{start}}$ and $\mathrm{vol_{start}}$ are the most important followed by μ and ξ. For the flow depth output, $\mathrm{vol_{start}}$ is the most relevant but its importance decreases along the path. At the end of the path from 2300m to 2412m where return periods are high (between 100 to 10 000 years), confidence intervals intersect. It seems

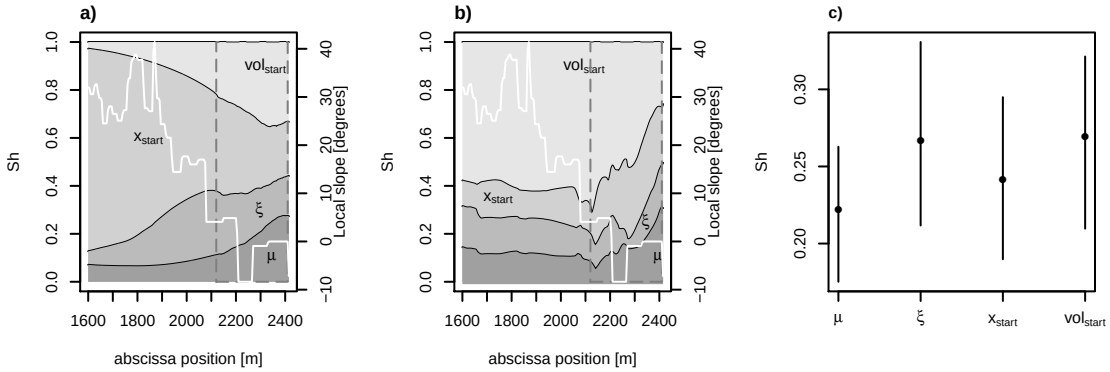

Figure 6: Avalanche model, scenario 1: a) and b) ubiquitous Shapley effects of velocity and flow depth curves, resp. and, c) runout distance Shapley effects. Shapley effects are estimated with a sample of size 6152 and Ntot=2002. The local slope is displayed with a white line. A gray dotted rectangle box is displayed at interval [2017, 2412] where snow avalanche return periods vary from 10 to 10 000 years. The bootstrap sample size is fixed to $B = 500$.

thus difficult to deduce a clear ranking of the inputs for these last portions of the path. Nevertheless, it seems that none of the inputs is negligible, even at the very end of the path. In summary, to estimate velocities with accuracy, the release zone and volume are the most important parameters and, for the flow depth, a good approximation of the volume released is essential.

6.3 Scenario 2

6.3.1 Principle

The aim is now to determine the most influential inputs in the context of strong knowledge regarding input distributions. In Eckert et al. [2010], the authors developed a Bayesian framework to estimate input distributions from available avalanche observations. The objective is long-term avalanche hazard assessment in order to assess the related risk for buildings and people inside. In the avalanche literature, it is assumed that ξ depends on the path topography, so it is a parameter and not a variable varying from one avalanche to another in Eckert et al. [2010]'s model. ξ is therefore fixed to its posterior estimate, 1300. Other input variables in this scenario are dependent. The dependence between $\mathrm{h_{start}}$ and $\mathrm{l_{start}}$ is modeled with a linear

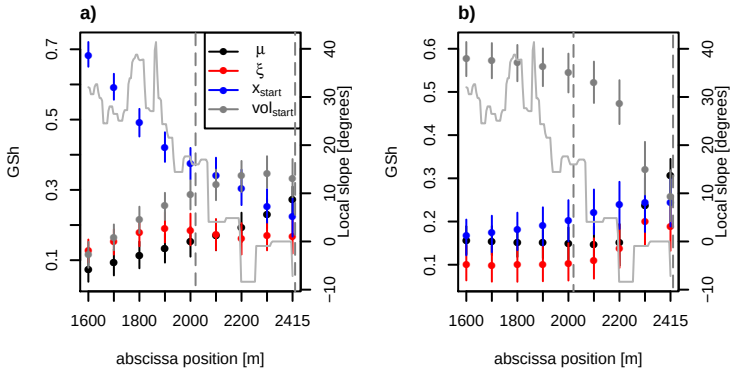

Figure 7: Avalanche model, scenario 1: a) and b) aggregated Shapley effects of velocity and flow depth curves calculated over space intervals $[x, 2412m]$ where $x \in \{1600m, 1700m, \ldots, 2412m\}$. Shapley effects are estimated with samples of size 6152 and Ntot=2002. Effects are estimated using the first fPCs explaining more than 95% of the output variance. The local slope is displayed with a gray line. A gray dotted rectangle is displayed at [2017m, 2412m] where snow avalanche return periods vary from 10 to 10 000 years. The bootstrap sample size is fixed to $B = 500$.

function $l_{start} = 31.25 + 87.5 h_{start}$, and similarly as in scenario 1, we consider vol_{start} as input of the GSA instead of h_{start} and l_{start}. The complete input distribution resulting from the Bayesian inference on the studied path is described in table 3. Input correlations have been computed. As an example, the correlation between μ and vol_{start} is 0.8. To perform the GSA in this scenario, our AR rules are: (i) avalanche is flowing in the interval [1600m, 2204m] where snow avalanche return periods vary from 10 to 300 years, (ii) avalanche volume is superior to 7,000 m^3 and, (iii) μ coefficient is inferior to 0.39 as we focus on dry snow avalanches. Under these conditions, we sample the full set of dry snow avalanches that could cause strong material or human damages on the studied site.

6.3.2 Global sensitivity analysis results

We first ran $n_0 = 100\,000$ avalanches from an i.i.d. sample of input distribution following table 3. After applying the AR algorithm, the sample size was reduced to $n_2 = 1284$ and the input distribution was modified. For example, μ and vol_{start} correlation changes from 0.8 to 0.2 which is still non negligible. Ubiquitous Shapley effects are displayed on section 6.3.2 pan-

Input	Distribution
$\mathrm{x_{nstart}} = \frac{x_{start}}{1600}$	$\mathrm{Beta}(1.38, 2.49)$
$\mathrm{h_{start}}\|x_{\mathrm{nstart}}$	$\mathrm{Gamma}\big(\frac{1}{0.45^2}(1.52+0.03x_{nstart})^2, \frac{1}{0.45^2}(1.52+0.03x_{nstart})\big)$
$\mathrm{l_{start}}$	$31.25{+}87.5\mathrm{h_{start}}$
$\mu\|h_{\mathrm{start}}, x_{\mathrm{nstart}}$	$\mathcal{N}(0.449 - 0.013x_{nstart} + 0.025h_{start}, 0.11^2)$

Table 3: Avalanche model: Scenario 2. Input description and uncertainty intervals. $\mathrm{x_{nstart}}$ is a normalization of $\mathrm{x_{start}}$. A linear relationship between $\mathrm{h_{start}}$ and $\mathrm{l_{start}}$ inferred from the local data is used Eckert et al. [2010]. In the the GSA, we consider $\mathrm{vol_{start}} = l_{start} \times h_{start} \times 72.3/\cos(35°)$ instead of $\mathrm{h_{start}}$ and $\mathrm{l_{start}}$.

els a and b. For the velocity, the three inputs have a similar importance till 1900m, then $\mathrm{vol_{start}}$ importance decreases and μ and $\mathrm{x_{start}}$ importance increases (see section 6.3.2 a). Similarly, as in scenario 1, the effects show fluctuations which correspond to changes in local slope. In particular, for the flow depth, input effects suffer radical changes when the local slope decreases from 20° to 10° (see section 6.3.2 b). For the runout distance, all inputs are relevant (see section 6.3.2 c).

Aggregated effects (see section 6.3.2) present less fluctuations and are easier to interpret (see section 6.3.2). In summary, under this second scenario, it is fundamental to have a good approximation of the released volume and abscissa for velocity forecasting, while for flow depth forecasting, a good approximation of released volume is desirable. Nevertheless, none of the other inputs are negligible. Note that the uncertainty associated to the estimation of Shapley effects at 2204m is high (see the width of the corresponding confidence intervals on section 6.3.2). To outperform the estimation accuracy at the end of the path generating a larger initial sample of avalanches is possible, but the computational burden is prohibitive.

7 Conclusions and perspectives

In this work, we extended Shapley effects to models with multivariate or functional outputs. We proved that aggregated Shapley effects accomplish the natural requirements for a GSA measure. For the estimation, we proposed to extend the subset aggregation procedure with double Monte Carlo given data estimator of Broto et al. [2020]. Also, we proposed an algorithm to construct bootstrap confidence intervals for scalar and aggregated Shapley

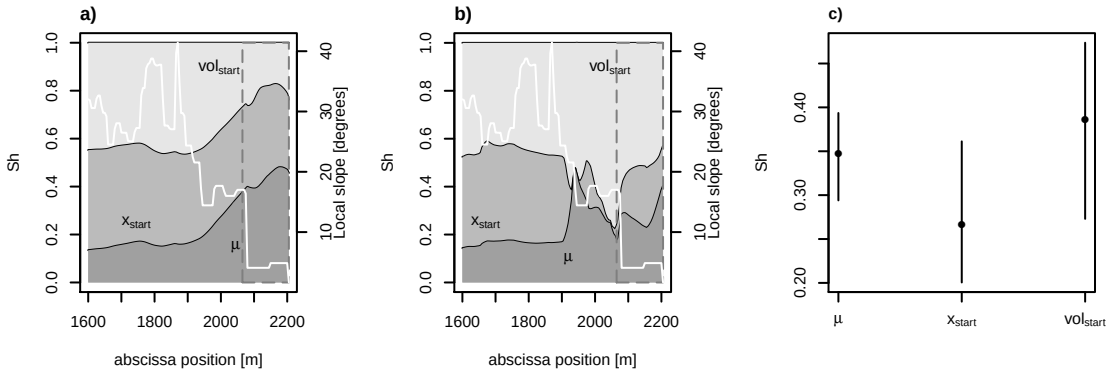

Figure 8: Avalanche model, scenario 2: a) and b) ubiquitous Shapley effects of velocity and flow depth curves, c) runout distance Shapley effects. Shapley effects are estimated with samples of size 1284 and Ntot=800. The local slope is displayed with a white line. A gray dotted rectangle shows the interval [2064, 2204] where return periods vary from 10 to 300 years. The bootstrap sample size is fixed to $B = 500$.

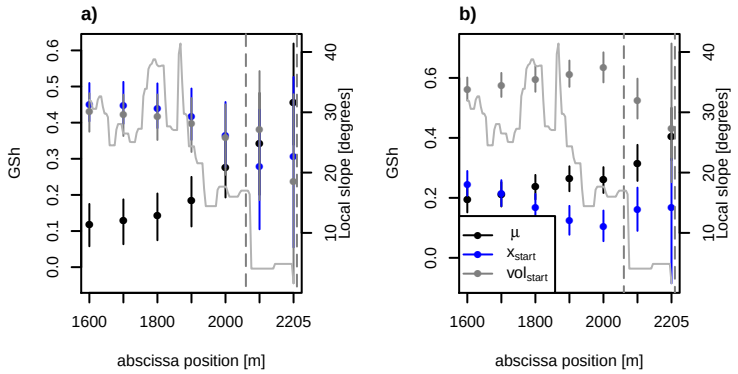

Figure 9: Avalanche model, scenario 2: a) and b) aggregated Shapley effects of velocity and flow depth curves calculated over space intervals $[x, 2204]$ where $x \in \{1600, 1700, \ldots, 2204\}$ and using the first fPCs which have 95% of output variance. Shapley effects are estimated with samples of size 1284 and Ntot=800. The local slope is displayed with a gray line. A gray dotted rectangle is displayed at [2017m, 2204m] where return periods vary from 10 to 300 years. The bootstrap sample size is fixed to $B = 500$.

effects based on the ideas of Benoumechiara, Nazih and Elie-Dit-Cosaque, Kevin [2019]. In test cases, the convergence of our estimator was empirically studied. Also, we proved empirically that the bootstrap confidence intervals we proposed have accurate coverage probability. Estimation and bootstrap confidence interval algorithms well behave. Nevertheless, high sample sizes ($n = 5000$ and $N_{tot} = 2002$) are required to guarantee accurate results. Remark that it is well known that Shapley effects estimation is costly. It would be interesting to study theoretically the asymptotic properties of our estimator, but this study is out of the scope of this paper. Recently, in the R package `sensitivity` the function `sobolshap_knn` to estimate Shapley effects with n and N_{tot} from a given data sample has been implemented. This function uses a tree based technique to approximate nearest-neighbor search which reduces drastically computation times. The function is particularly attractive if n and N_{tot} are high, we could even use $N_{tot} = (2^d - 2) \times n$. We did not use in the present work this function as we were not able to obtain confidence intervals with accurate coverage probability for the estimation it computes. We rather used the `shapleySubsetMc` function which corresponds to the estimator introduced in Broto et al. [2020] on which our estimator for aggregated Shapley effects is based.

We applied our GSA methods to an avalanche propagation model under two different settings. Model samples were obtained from an acceptance-rejection (AR) algorithm and input parameters were not confined in a rectangular region. For these reasons, it was not possible to consider independence of input parameters. Results showed probative linkages between local slope and sensitivity indexes. Notably, aggregated Shapley effects were more stable and easier to interpret than ubiquitous effects, as already observed by Alexanderian et al. [2020] in the case of aggregated Sobol' indices. This demonstrates the usefulness of our approach for many practical problems. Notably, it could be applied to other avalanche paths to generalize the results obtained in terms of respective weights of the inputs and interpret the sensitivity indices more deeply in terms of physical properties of avalanche flows. Eventually, application was challenging because AR samples were of moderate size, for example, from the 100 000 initial sample, the AR sampling produced a 6000 to 1200 sample, depending on the setting. In a future work, it would be useful to construct a surrogate of the avalanche model to generate larger AR samples, improve the accuracy of aggregated Shapley effect estimation and thus reduce confidence intervals width.

Acknowledgments

We thank Sébastien Da Veiga for fruitful discussions on nearest-neighbor estimation of Shapley effects. M.B. Heredia holds a Ph.D. grant from OSUG@2020 labex. Within the CDP-Trajectories framework, this work is supported by the French National Research Agency in the framework of the "Investissements d'avenir" program (ANR-15-IDEX-02). Part of the computations were performed using the Froggy platform of the CIMENT infrastructure (https://ciment.ujf-grenoble.fr), which is supported by the Rhône-Alpes region (GRANT CPER07 13 CIRA), the OSUG@2020 labex (reference ANR10 LABX56) and the Equip@Meso project (reference ANR-10-EQPX-29-01) of the program "Investissements d'avenir" supported by the Agence Nationale pour la Recherche.

References

Alen Alexanderian, Pierre A. Gremaud, and Ralph C. Smith. Variance-based sensitivity analysis for time-dependent processes. *Reliability Engineering & System Safety*, 196:106722, 2020. ISSN 0951-8320. doi: https://doi.org/10.1016/j.ress.2019.106722. URL `http://www.sciencedirect.com/science/article/pii/S0951832019303837`.

Anestis Antoniadis, Cline Helbert, Clmentine Prieur, and Laurence Viry. Spatio-temporal metamodeling for West African monsoon. *Environmetrics*, 23(1):24–36, 2012. doi: 10.1002/env.1134. URL `https://onlinelibrary.wiley.com/doi/abs/10.1002/env.1134`.

Isadora Antoniano-Villalobos, Emanuele Borgonovo, and Xuefei Lu. Nonparametric estimation of probabilistic sensitivity measures. *Statistics and Computing*, Aug 2019. ISSN 1573-1375. doi: 10.1007/s11222-019-09887-9. URL `https://doi.org/10.1007/s11222-019-09887-9`.

Benjamin Auder and Iooss B. Global sensitivity analysis based on entropy. In *In Safety, Reliability and Risk Analysis - Proceedings of the ESREL 2008 Conference*, pages 2107–2115. CRC Press, 2008.

P. Bartelt, Y. Bühler, O. Buser, M. Christen, and L. Meier. Modeling mass-dependent flow regime transitions to predict the stopping and depositional behavior of snow avalanches. *Journal of Geophysical Research (Earth Surface)*, 117(F1):F01015, February 2012. doi: 10.1029/2010JF001957.

Benoumechiara, Nazih and Elie-Dit-Cosaque, Kevin. Shapley effects for sensitivity analysis with dependent inputs: bootstrap and kriging-based algorithms. *ESAIM: ProcS*, 65:266–293, 2019. doi: 10.1051/proc/201965266. URL https://doi.org/10.1051/proc/201965266.

E. Borgonovo. A new uncertainty importance measure. *Reliability Engineering & System Safety*, 92(6):771 – 784, 2007. ISSN 0951-8320. doi: https://doi.org/10.1016/j.ress.2006.04.015. URL http://www.sciencedirect.com/science/article/pii/S0951832006000883.

Emanuele Borgonovo and Elmar Plischke. Sensitivity analysis: A review of recent advances. *European Journal of Operational Research*, 248(3): 869–887, 2016. doi: 10.1016/j.ejor.2015.06.032. URL https://doi.org/10.1016/j.ejor.2015.06.032.

Emanuele Borgonovo, Gordon B. Hazen, and Elmar Plischke. A Common Rationale for Global Sensitivity Measures and Their Estimation. *Risk Analysis*, 36(10):1871–1895, 2016. doi: 10.1111/risa.12555. URL https://onlinelibrary.wiley.com/doi/abs/10.1111/risa.12555.

E. Bourova, E. Maldonado, J.B. Leroy, R. Alouani, N. Eckert, M. Bonnefoy-Demongeot, and M. Deschatres. A new web-based system to improve the monitoring of snow avalanche hazard in France. *Natural Hazards and Earth System Sciences*, 16(5):1205–1216, 2016. doi: 10.5194/nhess-16-1205-2016. URL https://hal.archives-ouvertes.fr/hal-01507671.

W Brian Dade and Herbert E Huppert. Long-runout rockfalls. *Geological Society of America*, 26(9):803–806, 1998. doi: 10.1130/0091-7613(1998)026⟨0803:LRR⟩2.3.CO;2.

Baptiste Broto, Franois Bachoc, and Marine Depecker. Variance Reduction for Estimation of Shapley Effects and Adaptation to Unknown Input Distribution. *SIAM/ASA Journal on Uncertainty Quantification*, 8(2): 693–716, 2020. doi: 10.1137/18M1234631. URL https://doi.org/10.1137/18M1234631.

William B. Capra and Hans-Georg Müller. An accelerated-time model for response curves. *Journal of the American Statistical Association*, 92(437): 72–83, 1997. doi: 10.1080/01621459.1997.10473604. URL https://doi.org/10.1080/01621459.1997.10473604.

Gaelle Chastaing, Fabrice Gamboa, and Clémentine Prieur. Generalized Hoeffding-Sobol decomposition for dependent variables - application to sensitivity analysis. *Electron. J. Statist.*, 6:2420–2448, 2012. doi: 10.1214/12-EJS749. URL https://doi.org/10.1214/12-EJS749.

Yaqing Chen, Cody Carroll, Xiongtao Dai, Jianing Fan, Pantelis Z. Hadjipantelis, Kyunghee Han, Hao Ji, Hans-Georg Mueller, and Jane-Ling Wang. *fdapace: Functional Data Analysis and Empirical Dynamics*, 2020. URL https://CRAN.R-project.org/package=fdapace. R package version 0.5.1.

Sébastien Da Veiga and Fabrice Gamboa. Efficient estimation of sensitivity indices. *Journal of Nonparametric Statistics*, 25(3):573–595, September 2013. doi: 10.1080/10485252.2013.784.

Gregory Delipei. *Développement d'une méthodologie de Quantification d'Incertitudes pour une analyse Multi-Physique Best Estimate et application sur un Accident d'Éjection de Grappe dans un Réacteur à Eau Pressurisée*. PhD thesis, 2019. URL http://www.theses.fr/2019SACLX078. Thèse de doctorat dirigée par Garnier, Josselin Mathématiques appliquées Université Paris-Saclay (ComUE) 2019.

N. Eckert, E. Parent, and D. Richard. Revisiting statistical-topographical methods for avalanche predetermination: Bayesian modelling for runout distance predictive distribution. *Cold Regions Science and Technology*, 49(1):88 – 107, 2007. ISSN 0165-232X. doi: https://doi.org/10.1016/j.coldregions.2007.01.005. URL http://www.sciencedirect.com/science/article/pii/S0165232X07000080. Selected Papers from the General Assembly of the European Geosciences Union (EGU), Vienna, Austria, 25 April 2005.

N. Eckert, E. Parent, T. Faug, and M. Naaim. Optimal design under uncertainty of a passive defense structure against snow avalanches: from a general Bayesian framework to a simple analytical model. *Natural Hazards and Earth System Sciences*, 8(5):1067–1081, 2008a. doi: 10.5194/nhess-8-1067-2008. URL https://www.nat-hazards-earth-syst-sci.net/8/1067/2008/.

N. Eckert, E. Parent, M. Naaim, and D. Richard. Bayesian stochastic modelling for avalanche predetermination: from a general system framework to return period computations. *Stochastic Environmental Research and Risk Assessment*, pages 185–206, Feb 2008b. ISSN 1436-

3259. doi: 10.1007/s00477-007-0107-4. URL https://doi.org/10.1007/s00477-007-0107-4.

N. Eckert, M. Naaim, and E. Parent. Long-term avalanche hazard assessment with a Bayesian depth averaged propagation model. *Journal of Glaciology*, 56:563–586, October 2010. doi: 10.3189/002214310793146331.

Eckert, Nicolas, Naaim, Mohamed, Giacona, Florie, Favier, Philomène, Lavigne, Aurore, Richard, Didier, Bourrier, Franck, and Parent, Eric. Repenser les fondements du zonage règlementaire des risques en montagne " récurrents ". *La Houille Blanche*, (2):38–67, 2018. doi: 10.1051/lhb/2018019. URL https://doi.org/10.1051/lhb/2018019.

B. Efron and R. Tibshirani. Bootstrap Methods for Standard Errors, Confidence Intervals, and Other Measures of Statistical Accuracy. *Statist. Sci.*, 1(1):54–75, 02 1986. doi: 10.1214/ss/1177013815. URL https://doi.org/10.1214/ss/1177013815.

Bradley Efron. Nonparametric standard errors and confidence intervals. *Canadian Journal of Statistics*, 9(2):139–158, 1981. doi: 10.2307/3314608. URL https://onlinelibrary.wiley.com/doi/abs/10.2307/3314608.

Jianqing Fan and Irne Gijbels. *Local polynomial modelling and its applications*. Number 66 in Monographs on statistics and applied probability series. Chapman & Hall, London, 1996. ISBN 0412983214. doi: 10.1201/9780203748725.

P Favier, D Bertrand, N Eckert, and M Naaim. A reliability assessment of physical vulnerability of reinforced concrete walls loaded by snow avalanches. *Natural Hazards and Earth System Sciences*, 14(3):689–704, 2014a. doi: 10.5194/nhess-14-689-2014.

P. Favier, N. Eckert, D. Bertrand, and M. Naaim. Sensitivity of avalanche risk to vulnerability relations. *Cold Regions Science and Technology*, 108:163 – 177, 2014b. ISSN 0165-232X. doi: https://doi.org/10.1016/j.coldregions.2014.08.009. URL http://www.sciencedirect.com/science/article/pii/S0165232X14001426.

F. Gamboa, A. Janon, T. Klein, and A. Lagnoux. Sensitivity analysis for multidimensional and functional outputs. *ArXiv e-prints*, November 2013.

Fabrice Gamboa, Alexandre Janon, Thierry Klein, and Agnès Lagnoux. Sensitivity indices for multivariate outputs. *Comptes Rendus Mathematique*, 351(7):307 – 310, 2013. ISSN 1631-073X. doi: https://doi.

org/10.1016/j.crma.2013.04.016. URL http://www.sciencedirect.com/science/article/pii/S1631073X13000824.

Fabrice Gamboa, Pierre Gremaud, Thierry Klein, and Agnès Lagnoux. Global sensitivity analysis: a new generation of mighty estimators based on rank statistics. *arXiv preprint arXiv:2003.01772*, 2020.

Qiao Ge and Monica Menendez. Extending Morris method for qualitative global sensitivity analysis of models with dependent inputs. *Reliability Engineering & System Safety*, 162:28 – 39, 2017. ISSN 0951-8320. doi: https://doi.org/10.1016/j.ress.2017.01.010. URL http://www.sciencedirect.com/science/article/pii/S0951832017300625.

Joseph Hart and Pierre A. Gremaud. An approximation theoretic perspective of sobol' indices with dependent variables. *International Journal for Uncertainty Quantification*, 8(6):483–493, 2018. ISSN 2152-5080. doi: 10.1615/Int.J.UncertaintyQuantification.2018026498.

Rob J Hyndman. Computing and graphing highest density regions. *The American Statistician*, 50(2):120–126, 1996. doi: 10.2307/2684423.

Rob J. Hyndman and Han Lin Shang. Rainbow plots, bagplots, and boxplots for functional data. *Journal of Computational and Graphical Statistics*, 19 (1):29–45, 2010. doi: 10.1198/jcgs.2009.08158. URL https://doi.org/10.1198/jcgs.2009.08158.

Bertrand Iooss and Paul Lemaître. *A Review on Global Sensitivity Analysis Methods*, pages 101–122. Springer US, Boston, MA, 2015. ISBN 978-1-4899-7547-8. doi: 10.1007/978-1-4899-7547-8_5. URL https://doi.org/10.1007/978-1-4899-7547-8_5.

Bertrand Iooss and Clementine Prieur. Shapley effects for sensitivity analysis with correlated inputs: Comparisons with Sobol' indices, numerical estimation and applications. *International Journal for Uncertainty Quantification*, 9(5):493–514, 2019. ISSN 2152-5080. doi: 10.1615/Int.J.UncertaintyQuantification.2019028372.

Matthew Irwin and Zheng Wang. *Dynamic Systems Modeling*, pages 1–12. American Cancer Society, 2017. ISBN 9781118901731. doi: 10.1002/9781118901731.iecrm0074. URL https://onlinelibrary.wiley.com/doi/abs/10.1002/9781118901731.iecrm0074.

Julien Jacques, Christian Lavergne, and Nicolas Devictor. Sensitivity analysis in presence of model uncertainty and correlated inputs. *Reliability Engineering & System Safety*, 91(10):1126 – 1134, 2006. ISSN 0951-8320. doi: https://doi.org/10.1016/j.ress.2005.11.047. URL http://www.sciencedirect.com/science/article/pii/S0951832005002231. The Fourth International Conference on Sensitivity Analysis of Model Output (SAMO 2004).

Alexandre Janon, Maëlle Nodet, and Clémentine Prieur. Uncertainties assessment in global sensitivity indices estimation from metamodels. *International Journal for Uncertainty Quantification*, 4(1):21–36, 2014. doi: 10.1615/Int.J.UncertaintyQuantification.2012004291.

S. Kucherenko, S. Tarantola, and P. Annoni. Estimation of global sensitivity indices for models with dependent variables. *Computer Physics Communications*, 183(4):937 – 946, 2012. ISSN 0010-4655. doi: https://doi.org/10.1016/j.cpc.2011.12.020. URL http://www.sciencedirect.com/science/article/pii/S0010465511004085.

S. Kucherenko, O.V. Klymenko, and N. Shah. Sobol' indices for problems defined in non-rectangular domains. *Reliability Engineering & System Safety*, 167:218 – 231, 2017. ISSN 0951-8320. doi: https://doi.org/10.1016/j.ress.2017.06.001. URL http://www.sciencedirect.com/science/article/pii/S0951832016301363. Special Section: Applications of Probabilistic Graphical Models in Dependability, Diagnosis and Prognosis.

Matieyendou Lamboni, David Makowski, Simon Lehuger, Benoit Gabrielle, and Herv Monod. Multivariate global sensitivity analysis for dynamic crop models. *Field Crops Research*, 113(3):312 – 320, 2009. ISSN 0378-4290. doi: https://doi.org/10.1016/j.fcr.2009.06.007. URL http://www.sciencedirect.com/science/article/pii/S0378429009001531.

Matieyendou Lamboni, Hervé Monod, and David Makowski. Multivariate sensitivity analysis to measure global contribution of input factors in dynamic models. *Reliability Engineering & System Safety*, 96(4):450 – 459, 2011. ISSN 0951-8320. doi: https://doi.org/10.1016/j.ress.2010.12.002. URL http://www.sciencedirect.com/science/article/pii/S0951832010002504.

Genyuan Li, Herschel Rabitz, Paul E. Yelvington, Oluwayemisi O. Oluwole, Fred Bacon, Charles E. Kolb, and Jacqueline Schoendorf. Global

sensitivity analysis for systems with independent and/or correlated inputs. *The Journal of Physical Chemistry A*, 114(19):6022–6032, 2010. doi: 10.1021/jp9096919. URL https://doi.org/10.1021/jp9096919. PMID: 20420436.

Alfredo López-Benito and Ricardo Bolado-Lavín. A case study on global sensitivity analysis with dependent inputs: The natural gas transmission model. *Reliability Engineering & System Safety*, 165:11 – 21, 2017. ISSN 0951-8320. doi: https://doi.org/10.1016/j.ress.2017.03.019. URL http://www.sciencedirect.com/science/article/pii/S0951832017303447.

Thierry A. Mara and Stefano Tarantola. Variance-based sensitivity indices for models with dependent inputs. *Reliability Engineering & System Safety*, 107:115 – 121, 2012. ISSN 0951-8320. doi: https://doi.org/10.1016/j.ress.2011.08.008. URL http://www.sciencedirect.com/science/article/pii/S0951832011001724. SAMO 2010.

Thierry A. Mara, Stefano Tarantola, and Paola Annoni. Non-parametric methods for global sensitivity analysis of model output with dependent inputs. *Environmental Modelling & Software*, 72:173 – 183, 2015. ISSN 1364-8152. doi: https://doi.org/10.1016/j.envsoft.2015.07.010. URL http://www.sciencedirect.com/science/article/pii/S1364815215300153.

M. Naaim. Dense avalanche numerical modeling: interaction between avalanche and structures. In *25 years of snow avalanche research, Voss, NOR, 12-16 May 1998*, pages 187–191, Norway, 1998. URL https://hal.inrae.fr/hal-02582417.

Mohamed Naaim, Florence Naaim-Bouvet, Thierry Faug, and Alexi Bouchet. Dense snow avalanche modeling: flow, erosion, deposition and obstacle effects. *Cold Regions Science and Technology*, 39(2):193 – 204, 2004. ISSN 0165-232X. doi: https://doi.org/10.1016/j.coldregions.2004.07.001. URL http://www.sciencedirect.com/science/article/pii/S0165232X04000643. Snow And Avalanches: Papers Presented At The European Geophysical Union Conference, Nice, April 2003. Dedicated To The Avalanche Dynamics Pioneer Dr. B. Salm.

Mohamed Naaim, Thierry Faug, Florence Naaim, and Nicolas Eckert. Return period calculation and passive structure design at the Taconnaz avalanche path, France. *Annals of Glaciology*, 51(54):89–97, 2010. doi: 10.3189/172756410791386517.

A. Owen. Sobol' Indices and Shapley Value. *SIAM/ASA Journal on Uncertainty Quantification*, 2(1):245–251, 2014. doi: 10.1137/130936233. URL https://doi.org/10.1137/130936233.

Art B. Owen and Clémentine Prieur. On Shapley value for measuring importance of dependent inputs. *SIAM/ASA Journal on Uncertainty Quantification*, 5(1), March 2017. URL https://doi.org/10.1137/16M1097717.

Elmar Plischke. An effective algorithm for computing global sensitivity indices (EASI). *Reliability Engineering & System Safety*, 95(4):354 – 360, 2010. ISSN 0951-8320. doi: https://doi.org/10.1016/j.ress.2009.11.005. URL http://www.sciencedirect.com/science/article/pii/S0951832009002579.

Elmar Plischke, Emanuele Borgonovo, and Curtis L. Smith. Global sensitivity measures from given data. *European Journal of Operational Research*, 226(3):536–550, 2013. doi: 10.1016/j.ejor.2012.11.06.

Elmar Plischke, Giovanni Rabitti, and Emanuele Borgonovo. Computing Shapley Effects for Sensitivity Analysis. *arXiv e-prints*, art. arXiv:2002.12024, February 2020.

Giovanni Rabitti and Emanuele Borgonovo. A Shapley–Owen index for interaction quantification. *SIAM/ASA Journal on Uncertainty Quantification*, 7(3):1060–1075, 2019. doi: 10.1137/18M1221801. URL https://doi.org/10.1137/18M1221801.

Majdi I. Radaideh, Stuti Surani, Daniel OGrady, and Tomasz Kozlowski. Shapley effect application for variance-based sensitivity analysis of the few-group cross-sections. *Annals of Nuclear Energy*, 129:264 – 279, 2019. ISSN 0306-4549. doi: https://doi.org/10.1016/j.anucene.2019.02.002. URL http://www.sciencedirect.com/science/article/pii/S0306454919300714.

John A. Rice and B. W. Silverman. Estimating the mean and covariance structure nonparametrically when the data are curves. *Journal of the Royal Statistical Society: Series B (Methodological)*, 53(1):233–243, sep 1991. doi: 10.1111/j.2517-6161.1991.tb01821.x. URL https://doi.org/10.1111%2Fj.2517-6161.1991.tb01821.x.

Romain Schläppy, Nicolas Eckert, Vincent Jomelli, Markus Stoffel, Delphine Grancher, Daniel Brunstein, Mohamed Naaim, and Michaël Deschatres. Validation of extreme snow avalanches and related return peri-

ods derived from a statistical-dynamical model using tree-ring techniques. *Cold Regions Science and Technology*, 99:12 – 26, 2014. ISSN 0165-232X. doi: https://doi.org/10.1016/j.coldregions.2013.12.001. URL http://www.sciencedirect.com/science/article/pii/S0165232X13001900.

L. Shapley. A Value for n-Person Games. *Contributions to the Theory of Games (AM-28), Princeton: Princeton University Press.*, 2, 1953. ISSN 307-318.

I. M. Sobol'. Sensitivity analysis for non-linear mathematical models. *Mathematical Modelling and Computational Experiment*, 1(4):407–414, 1993.

Maikol Solís. Non-parametric estimation of the first-order Sobol indices with bootstrap bandwidth. *Communications in Statistics - Simulation and Computation*, 0(0):1–16, 2019. doi: 10.1080/03610918.2019.1655575. URL https://doi.org/10.1080/03610918.2019.1655575.

E. Song, B. Nelson, and J. Staum. Shapley effects for global sensitivity analysis: Theory and computation. *SIAM/ASA Journal on Uncertainty Quantification*, 4(1):1060–1083, 2016. doi: 10.1137/15M1048070. URL https://doi.org/10.1137/15M1048070.

Yunpeng Sun, Daniel W. Apley, and Jeremy Staum. Efficient nested simulation for estimating the variance of a conditional expectation. *Operations Research*, 59(4):998–1007, 2011. doi: 10.1287/opre.1110.0932. URL https://doi.org/10.1287/opre.1110.0932.

Sebastien Da Veiga. Global sensitivity analysis with dependence measures. *Journal of Statistical Computation and Simulation*, 85(7):1283–1305, 2015. doi: 10.1080/00949655.2014.945932. URL https://doi.org/10.1080/00949655.2014.945932.

Chonggang Xu. Decoupling correlated and uncorrelated parametric uncertainty contributions for nonlinear models. *Applied Mathematical Modelling*, 37(24):9950 – 9969, 2013. ISSN 0307-904X. doi: https://doi.org/10.1016/j.apm.2013.05.036. URL http://www.sciencedirect.com/science/article/pii/S0307904X13003570.

Chonggang Xu and George Zdzislaw Gertner. Uncertainty and sensitivity analysis for models with correlated parameters. *Reliability Engineering & System Safety*, 93(10):1563 – 1573, 2008. ISSN 0951-8320. doi: https://doi.org/10.1016/j.ress.2007.06.003. URL http://www.sciencedirect.com/science/article/pii/S0951832007001652.

Fang Yao, Hans-Georg Müller, and Jane-Ling Wang. Functional data analysis for sparse longitudinal data. *Journal of the American Statistical Association*, 100(470):577–590, 2005. doi: 10.1198/016214504000001745. URL https://doi.org/10.1198/016214504000001745.

Kaichao Zhang, Zhenzhou Lu, Lei Cheng, and Fang Xu. A new framework of variance based global sensitivity analysis for models with correlated inputs. *Structural Safety*, 55:1 – 9, 2015. ISSN 0167-4730. doi: https://doi.org/10.1016/j.strusafe.2014.12.005. URL http://www.sciencedirect.com/science/article/pii/S0167473015000181.